Icarus **142**, 498–508 (1999)
Article ID icar.1999.6215, available online at http://www.idealibrary.com on IDEAL®

Infrared Spectroscopy of the ν_3 Band of Hydrogen Cyanide in Comet C/1995 O1 Hale–Bopp

Karen Magee-Sauer

Department of Chemistry and Physics, Rowan University, Glassboro, New Jersey 08028
E-mail: sauer@rowan.edu

Michael J. Mumma

Laboratory for Extraterrestrial Physics, NASA Goddard Space Flight Center Code 690, Greenbelt, Maryland 20771

Michael A. DiSanti and Neil Dello Russo

Laboratory for Extraterrestrial Physics, NASA Goddard Space Flight Center Code 690, Greenbelt, Maryland 20771; and Department of Physics, The Catholic University of America, Washington DC 20064

and

Terrence W. Rettig

Department of Physics and Astronomy, University of Notre Dame, Notre Dame, Indiana 46556

Received March 22, 1999; revised August 16, 1999

Hydrogen cyanide (HCN) was detected in Comet Hale–Bopp at infrared wavelengths near 3.0 μm on four dates between Feb 24.0 and May 1.0 1997 using high-resolution spectroscopy. The average rotational temperature retrieved for the (001) vibrational level on UT 1997 April 29.9 was (95 ± 6) K near the nucleus, increasing to (122 ± 8) K in the intermediate coma (4″–10″ off the nucleus). The HCN production rate on April 29.9 was $(3.09 \pm 0.13) \times 10^{28}$ molecules s^{-1}. When compared with the water production rate obtained from direct measurements of the H_2O 100-010 band on common observation dates using the same instrument and data processing algorithms, the weighted average (for the four dates) of the relative abundance (HCN/H_2O) was (0.40 ± 0.05)%. The measured spatial distribution for HCN is consistent with its release at the nucleus—no significant contribution from a distributed source is required within 10,000 km of the nucleus.

Key Words: **comets, Hale–Bopp; composition; infrared observations; hydrogen cyanide.**

INTRODUCTION

Hydrogen cyanide (HCN) is a key intermediary for synthesis of biochemical compounds on Earth—its presence in monomeric and/or polymeric form in liquid water can lead to amino acid formation, without which life as we know it would not exist (Oro 1961, Oro *et al*. 1992). A tetramer of HCN (diaminomaleonitrile) may have played a key role in prebiotic chemical evolution on Earth (Ferris and Hagan 1984). Yet Earth formed in a hot nebular region (∼1000 K, cf. Boss 1998), where preplanetary solids were depleted in the low-Z elements (e.g., H, C, N, O) normally found in ices and low temperature organic refractories (McKay 1991). These elements (and HCN) would have been severely underabundant on early Earth had not some later enhancement occurred. A current view is that Earth's volatile inventory was enriched by infall of comets, asteroids, and interplanetary dust during the late heavy bombardment phase of the early Solar System (cf. Chyba *et al*. 1994).

Comets such as Hale–Bopp formed in the Jupiter–Neptune region where low temperatures permitted them to retain "native" frozen volatiles (cf. Mumma *et al*. 1993). They later were ejected by the growing giant planets, and those which formed the Oort cloud remained in the distant Solar System until being injected again into the planetary region, reappearing as dynamically "new" comets. After a few passes through the planetary region, they can be perturbed into orbits such as that of Comet Hale–Bopp. Because they never experienced high temperatures, the interiors of these cometary nuclei are thought to retain their natal ices. If so, they are the least modified bodies remaining from the formative phase of the Solar System. Their present composition and structure represent a fingerprint of chemical and physical conditions during their formation, which provide clues as to the types of material brought to prebiotic Earth by comets and interplanetary dust, bodies which carry a variety of organic ices and dust (Mumma *et al*. 1993, Mumma 1997,

0019-1035/99 $30.00

Schulze *et al*. 1997). The survival of specific chemicals from the largest impactors depends on detailed processes during the collision (Chyba and Sagan 1992), but many small bodies reach Earth's surface intact. Analysis of carbonaceous chondrites (the most primitive meteorites) and of interplanetary dust particles (comet debris) shows that small bodies deliver an inventory of exogenous complex organics to Earth's surface even today (Clemett *et al*. 1993, Cronin and Chang 1993).

The form and abundance of hydrogen cyanide in comets is of particular interest in the context of exogenous delivery of this key prebiotic chemical. HCN is a known component in comets and is thought to be present as a native ice in the cometary nucleus—a so-called "parent" species—where it could exist in both monomeric and polymeric forms. Its abundance relative to other nitrogen bearing species (e.g., NH_3, N_2) can indicate the temperature of formation and the kind and degree of processing experienced by precometary material, whether in the natal cloud or in the solar nebula (Mumma *et al*. 1993). If monomeric HCN were sufficiently abundant in native cometary ice, a polymeric or oligomeric form could coexist there or could form during warming (Rettig *et al*. 1992). Hydrogen cyanide readily forms linear hydrogen-bonded addition polymers (Pauling 1960, Pimentel and McClellan 1960), which could provide a distributed source of HCN monomers if carried into the coma. The presence of a distributed source for HCN could imply the release of addition polymers of HCN, release of hydrogen-bonded heterodimers such as $H_2O : HCN$, or production of HCN monomers by chemistry in the coma. In the presence of a base (e.g., NH_3, N_2H_4), HCN can also reorder into valence-bonded oligomers (Völker 1960). Being less volatile than the monomer and addition polymers, HCN oligomers could reside on the surface of a comet nucleus for long intervals (Matthews and Ludicky 1992) or be carried far into the coma before dissociating. Oligomers such as biologically significant diaminomaleonitrile ($(HCN)_4$) could provide a distributed source of NH_2, C_2, and CN (Huebner *et al*. 1989) but not of HCN itself. Thus, the spatial distribution of HCN in the coma may indicate the nature of its sources, and its abundance can provide limits for production of the CN daughter species observed extensively at optical wavelengths (Bockelée-Morvan and Crovisier 1985).

In this paper we report spectroscopic observations of HCN in C/1995 O1 Hale–Bopp at infrared wavelengths near 3.0 μm. From them, we obtain the absolute production rate of HCN and its spatial distribution in the coma, along with the rotational temperature and its spatial variation. We use these data to obtain insights regarding the release of HCN from this comet.

BACKGROUND

HCN emits radiation in millimeter and infrared regions via rotational and rovibrational transitions, respectively. A detection of cometary HCN was first claimed at millimeter wavelengths in Comet Kohoutek 1973 XII (Huebner *et al*. 1974), and upper limits of its abundance were obtained for numerous comets thereafter (Bockelée-Morvan *et al*. 1984, Irvine *et al*. 1984). HCN was first securely detected in Comet 1P/Halley and was studied extensively throughout that apparition (Despois *et al*.1986, Bockelée-Morvan *et al*. 1986, 1987, Schloerb *et al*. 1987, Winnberg *et al*. 1987), confirming HCN as a progenitor for some but not all of the CN observed at optical wavelengths. After Halley, HCN was detected and characterized in numerous comets (Bockelée-Morvan *et al*. 1990, 1994, Crovisier *et al*. 1993, Palmer *et al*. 1990, Wootten *et al*. 1994). However, these measurements were all made at low spatial resolutions so they shed little light on the distribution of HCN within the inner coma or on mechanisms responsible for its release.

In Hale–Bopp, many groups observed and tracked HCN production at millimeter wavelengths (Biver *et al*. 1997, 1999, Despois 1999, Lis *et al*. 1997, Lovell *et al*. 1998, Rauer *et al*. 1996, Schloerb *et al*. 1996, Womack *et al*. 1998, Woodney *et al*. 1998). The distribution of HCN was mapped using both single aperture telescopes (Lovell *et al*. 1998, Womack *et al*. 1998) and interferometers (Bockelée-Morvan *et al*. 1998, Veal *et al*. 1998, Wright *et al*. 1998), providing the potential for separately identifying native and distributed sources for HCN on spatial scales larger than the respective instrumental resolutions. These spatial resolutions ranged from 15–20 arcsec for single aperture telescopes to 10 arcsec for the BIMA array and 3–4 arcsec at the IRAM Plateau de Bure Interferometer.

Improved spatial resolution can be obtained at infrared wavelengths, owing to the linear decrease in diffraction limit with wavelength for comparably sized telescopes. Prospects for detecting cometary HCN through vibrational infrared fluorescence were explored by Crovisier (1987). For a time, sensitive searches were not possible, but recent advances in instrumentation enabled detection of HCN at infrared wavelengths in Comets C/1996 B2 Hyakutake and C/1995 O1 Hale–Bopp (Brooke *et al*. 1996, 1998, Magee-Sauer *et al*. 1997, 1998, Mumma *et al*. 1996, Weaver *et al*. 1999).

OBSERVATIONS AND RESULTING SPECTRA

We obtained spectroscopic observations of C/1995 O1 Hale–Bopp using the CSHELL cryogenic echelle grating spectrometer (Greene *et al*. 1993) at the NASA Infrared Telescope Facility on Mauna Kea, Hawaii. CSHELL incorporates a 256×256 InSb array detector having $0.2''$ pixels. The slit ($1'' \times 30''$) corresponds to spatial dimensions of approximately $725^*\Delta$ km in width and $21{,}800^*\Delta$ km in length (oriented east–west) at the comet (Δ is the geocentric distance, in AU). Acquired frames contain spectral–spatial images of cometary emissions. These provide spatially resolved spectra at a spectral resolving power of approximately $\nu/\Delta\nu \sim 2 \times 10^4$ (when the source fills the slit), sufficient to resolve individual cometary emission lines. The intensity profile of cometary emissions along the slit provides the information needed to separate direct (nuclear) and distributed sources. Although recorded at $0.2''$ per pixel, the data were later

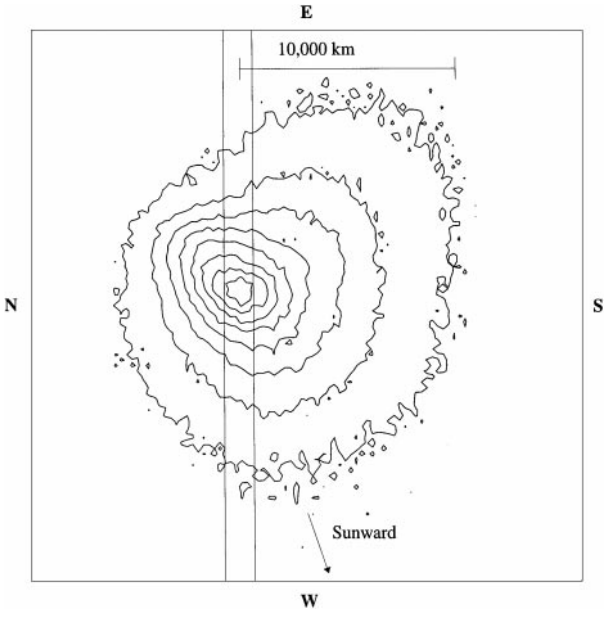

FIG. 1. Comet Hale–Bopp imaged through a 3.5-μm CVF on UT 1997 April 29.9. Contours represent increments of 400 counts/s (1 count/s = $\sim 1 \times 10^{-19}$ Watts/m^2/cm^{-1}). The $1'' \times 30''$ second slit was centered at the position of the brightest cometary emission through the CVF. For this date ($\Delta = 1.753$ AU), the width of the slit was 1270 km.

binned to a spatial resolution of $1''$ or more to improve the signal-to-noise ratio.

Most observations occurred during daytime when the telescope's autoguiding capability was not useable, so we centered the comet within the slit by imaging at 3.5 μm through a circular variable filter (CVF) (Fig. 1). The comet's position was checked and updated by imaging at regular intervals, and these images document the general morphology of the dust flow during the observations. Guide rates were continually upgraded with these measurements; although not perfect, tracking of the comet throughout the course of a frame was acceptable within the limits of atmospheric seeing. Spectra were acquired at each grating setting by taking two frames with the slit centered on the comet ("a") and two with the slit displaced $120''$ off the comet ("b"), in an "abba" sequence. Each sequence was immediately followed by flat fields (using an internal continuum lamp) and dark frames. Exposure times on source were typically limited to 60 s per frame to minimize cometary drift during the sequence. Absolute flux calibration of the cometary spectra was achieved using observations of infrared flux standard stars through a $4''$ slit to ensure inclusion of the total stellar flux.

First order processing of the data included sky subtraction, flat fielding, removal of high dark current pixels and cosmic ray hits, and removal of floating bias current. Curvature of the CSHELL optics causes the spectrum to droop from left to right. This was corrected column-by-column, so that a spatial position on the sky fell along a single row of the detector. Also, the dispersion varied from top-to-bottom on the frame. Atmospheric emission lines were used to measure the absolute spectral calibration along each row, and the cometary frame was resampled row-by-row to provide uniform dispersion over the length of the slit. Individual "a minus b" frames (representing net comet signal) were shifted to a common detector row and coadded to improve the signal-to-noise ratio for each grating setting. We used the Spectrum Synthesis Program (Kunde and Maguire 1974), which accesses the HITRAN 1992 molecular data base (Rothman *et al*. 1992), to establish an absolute frequency scale and to model the fully resolved transmittance spectrum of the terrestrial atmosphere. We generated a 20-layer model atmosphere with appropriate temperature and pressure profiles using column burdens of absorbing gases matched to those observed in the comet spectrum. The optimized model was binned to the spectral resolution of the cometary spectrum and normalized to the continuum level. Cometary molecular emissions were obtained by subtracting this normalized synthetic continuum model from the comet spectrum (cf Fig. 2). The true line flux at the top of the atmosphere was obtained by dividing the total flux of the cometary emission line by the fully resolved atmospheric transmittance at the Doppler-shifted line position.

We detected numerous rovibrational spectral lines of the ν_3 band of HCN on multiple dates (Table I). The spectral grasp of each grating setting spans three rovibrational lines of the ν_3 band of HCN, so four grating settings were needed to adequately sample its rotational population distribution. Spectra were extracted from the processed frames by coadding five rows centered on the nucleus, for each of the four grating settings (Figs. 2A–2D). Due to the high continuum levels exhibited in Comet Hale–Bopp, cometary emission lines are more easily recognized after continuum subtraction. However, care must be exercised when interpreting residuals in the cores of the strong atmospheric lines where the model may not adequately represent the cometary continuum and atmospheric spectral emission leads to increased noise. The 3-μm region is rich in cometary molecular line emissions. Other species detected in these spectra (e.g., C_2H_2, NH_2, OH, and NH_3) will be reported elsewhere.

Several unidentified emissions appear in our spectra (Fig. 2A). These unknown features are consistently present in all spectra in both comets Hale–Bopp and Hyakutake (Magee-Sauer *et al*. 1998) and typically display intensities comparable to HCN emissions. A search of several molecular data bases determined that the emissions could not be attributed to molecules included there. Infrared transitions from species newly discovered at

TABLE I
HCN Detections in Hale–Bopp

Date(s) (UT 1997)	r_h (AU)	Δ (AU)	HCN lines detected
Feb. 24.0	1.114	1.567	P2, P3, P4, P6, P7
April 6.1	0.918	1.397	P2, P3, R6
April 29.9	1.047	1.753	P2, P3, P4, P7, P8, P11, R6, R7
May 1.0	1.057	1.770	P3, P4, P5, P7

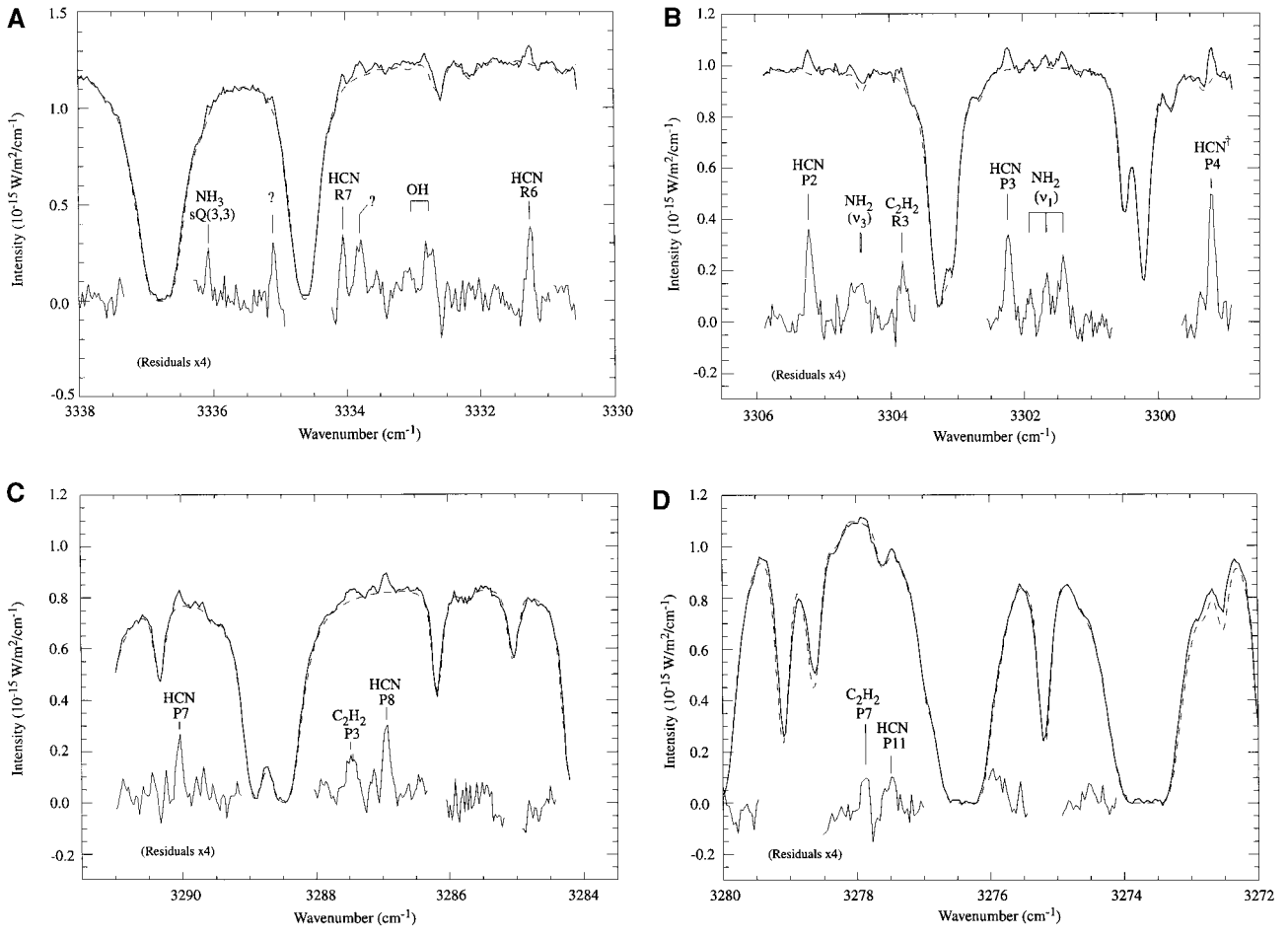

FIG. 2. Flux-calibrated spectra of Comet Hale–Bopp for four grating settings obtained on UT 1997 April 29.9. Each figure shows cometary continuum and molecular emission lines (solid curve), normalized atmospheric transmittance spectrum (dashed line), and their difference (multiplied by four). As seen in (A)–(D) the 3-μm region is rich in cometary molecular line emissions. HCN, C_2H_2, OH, NH_2, NH_3, and unknown species were detected. †The HCN P4 line includes a minor contribution from the R1 rovibrational line of C_2H_2.

millimeter wavelengths (Bockelée-Morvan *et al.* 1999) were carefully considered and eliminated. The spatial profiles of the unidentified emissions were consistent with a parent volatile distribution. The fact that the emissions were relatively bright suggested that the product of column density and fluorescence efficiency for the unknown species must be comparable to that of HCN. Possibilities range from a strong band of a comparably abundant species to a weak band of a more abundant species. Frequencies for lines from several weak "hot" bands of H_2O were obtained using the combination of differences method, and many lines fall in the 3-μm region. Our two strongest emissions are preliminarily consistent with the $2\nu_1 - \nu_1$ band of H_2O, however more complete band modeling is needed to permit a secure identification.

ROTATIONAL TEMPERATURES

To obtain a production rate for HCN, it is first necessary to determine its effective rotational temperature at each position along the slit. For a simple linear molecule such as HCN, the relative intensity of each rovibrational line in emission is given by

$$I_{\rm em} = \frac{C_{\rm em}}{Q_{\rm r}} N_{001} \nu^4 (J' + J'' + 1) e^{-B'J'(J'+1)hc/(kT)},$$

where ν is the frequency of the transition (cm^{-1}), J' and J'' are the upper and lower rotational quantum numbers respectively, B' is the rotational constant of the (001) vibrational level, $C_{\rm em}$ is a geometrical constant, $Q_{\rm r}$ is the rotational partition function of the molecule, and N_{001} is the column density in the (001) vibrational level (Herzberg 1950). We take $B' = B'' = 1.47$ cm^{-1}. The effective rotational temperature (T) in the (001) level of HCN is readily determined by comparing (k/hcB') $\ln[(I_{\rm em}/\nu^4\ (J' + J'' + 1)]$ against $J'(J' + 1)$ for the lines observed. A weighted least squares linear fit has a slope of $-1/T$.

Eight rovibrational lines of HCN were measured on UT 1997 April 29.9 within approximately a one hour time interval

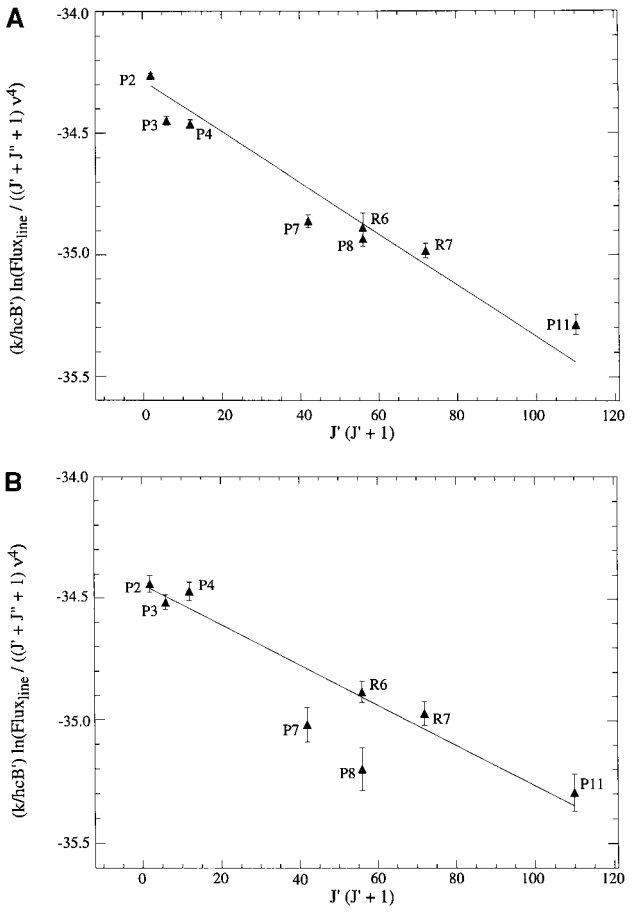

FIG. 3. Rotational temperature analysis for 8 rovibrational lines of HCN on UT 1997 April 29.9. (A) Line intensities extracted from a $1'' \times 1''$ box centered on the nucleus. (B) Line intensities extracted from a region extending $4''$–$10''$ from the comet nucleus. The retrieved rotational temperature (Trot) was 95 ± 6 K for the nuclear centered extracts and increased to 122 ± 8 K for the $4''$–$10''$ region. The intensity of the P4 line includes a minor contribution from the R1 rovibrational line from C_2H_2. If the P4 line is omitted from the fit, the retrieved temperature does not change for nuclear centered extracts and increases by 3 K for the $4''$–$10''$ extract.

(minimizing possible temporal variability). A spatial profile was obtained for an individual emission line by summing over its spectral extent in a processed cometary frame. The resulting "strip" included cometary line emission, dust continuum, and uncanceled sky (if any). The cometary molecular line emission was isolated by subtracting another strip which included only continuum; corrections were applied when the atmospheric transmittance and/or residual background levels differed for the two strips. Line intensities and rotational analyses for two positions are shown in Fig. 3, and derived rotational temperatures are shown in Table II.

A similar approach was used for regions displaced in both eastward and westward directions from the nucleus, but reliable rotational temperatures within a $1'' \times 1''$ aperture could be retrieved only within 3 arcsec of the nucleus, owing to signal-to-noise considerations (Table II, Fig. 4). Our results suggest that the rotational temperature increases in each direction to around $3''$ from the nucleus, as expected if thermalization of fast H atoms produced by photolysis of H_2O and/or electron collisions heated the coma in this region (cf. Bockelée-Morvan and Crovisier 1987, Xie and Mumma 1992). We see a similar effect for CO on multiple dates (DiSanti *et al*. 1999). Rotational temperatures obtained for HCN on other dates for $1'' \times 1''$ regions centered on the nucleus are consistent with the results for UT 1997 April 29.9, however the uncertainties are larger because fewer lines were measured on those dates (Table I, Table III).

TABLE II
Spatial Dependence of Rotational Temperature of the ν_3 Band of HCN (UT Date 1997 April 29.9)

Offset[a]	Average east/west	East of nucleus	West of nucleus
$0''$	95 ± 6	—	—
$1''$	107 ± 10	109 ± 5	100 ± 4
$2''$	120 ± 14	133 ± 10	111 ± 6
$3''$	123 ± 15	129 ± 14	129 ± 12
$4''$–$10''$	122 ± 8		

[a] Rotational temperatures are extracted using fluxes in a $1'' \times 1''$ box centered at the offset distance. The final entry ($4''$–$10''$) is derived using the weighted average of the combined fluxes in a region extending $4''$–$10''$ from the nucleus.

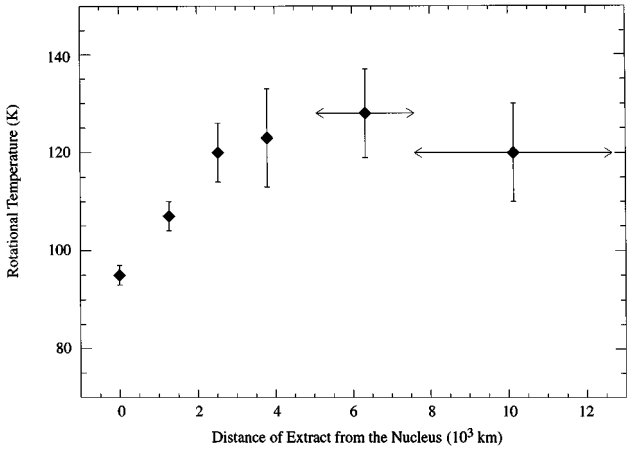

FIG. 4. Retrieved rotational temperatures (Trot) as a function of line-of-sight distance from the nucleus. Each point represents the retrieved Trot from average line intensities extracted using a $1'' \times 1''$ box at positions of 0, $\pm 1''$, $\pm 2''$, $\pm 3''$ from the nuclear centered position. Outside of $3''$ ($\sim$4000 km), the box size increased to include a region $4''$–$6''$ and $6''$–$10''$ from the nuclear centered position. The retrieved Trot increases with distance from the nucleus, as expected if thermalization of fast H atoms produced by photolysis of H_2O and/or electron collisions heated the coma in this region (Xie and Mumma 1992). The error shown for each point is the stochastic error. A systematic error contributes an additional uncertainty of $\sim$10 K to each retrieved Trot and is the same for each offset.

TABLE III
HCN Production Rates and Rotational Temperatures in C/1995 Hale–Bopp

Date 1997 (UT)	T_0rot[a] (K)	β_0^b (%)	T_{4-10}rot[c] (K)	β_{4-10}^d (%)	F^e (10^{-17} W m^{-2})	$Q_{\rm HCN}^f$ (10^{28} mol s^{-1})	$Q_{\rm HCN}/Q_{\rm H20}^g$ (%)
Feb. 24.0	95 ± 10	29	120[h]	25	8.5	2.39 ± 0.20	0.27 ± 0.04[i]
April 6.1	97 ± 18	14	120[h]	12	14	5.62 ± 0.54	0.53 ± 0.07
April 29.9	95 ± 6	38	122 ± 8	36	13	3.09 ± 0.13	0.46 ± 0.03
May 1.0	98 ± 12	25	120[h]	22	7.1	2.80 ± 0.36	0.38 ± 0.05

[a] The rotational temperature retrieved for a $1'' \times 1''$ region centered on the comet nucleus for the (001) vibrational level.
[b] β_0 is the modeled fraction of the total ν_3 band represented by the lines measured for the date in question, assuming a rotational temperature of T_0rot.
[c] The mean rotational temperature for a region extending $4''$–$10''$ from the comet nucleus for the (001) vibrational level.
[d] β_{4-10} is the modeled fraction of the total ν_3 band represented by the lines measured for the date in question, assuming a rotational temperature of T_{4-10}rot.
[e] F is the total emission flux along the slit between $2''$–$10''$ (averaged east–west) from the comet nucleus for all the lines measured on a particular date (representing a fraction β of the total ν_3 band).
[f] $Q_{\rm HCN}$ (global production rate) for a region $2''$–$10''$ from the nucleus. The global HCN production rates are slightly overestimated due to a minor contribution from the R1 C_2H_2 rovibrational line to the P4 line of HCN. However, the same HCN production rate is retrieved within the experimental error if the P4 line is omitted from our analysis. We estimate the correction to the total HCN production rate to be less than 2% for a rotational temperature of 120 K and $Q_{\rm C2H2}/Q_{\rm H2O} \sim 0.2\%$. The exact contribution will be determined in future work.
[g] $Q_{\rm H2O}$ from measured values (Dello Russo *et al*. 1999).
[h] Adopted temperature.
[i] The measured $Q_{\rm H2O}$ on Feb. 24.0 is significantly higher than predicted by the water production evolution curve derived in Dello Russo *et al*. ($Q_{\rm H2O} = (8.35 \pm 0.13) \times 10^{30}[R_{\rm h}^{(-1.88\pm0.18)}]$). If the evolution curve value is used, the relative abundance ($Q_{\rm HCN}/Q_{\rm H2O}$) is 0.35 ± 0.04.

SPATIAL PROFILES AND PRODUCTON RATES

The "spatial profile" for line or continuum emission is a measure of the distribution of intensity along the slit (Dello Russo *et al*. 1998, DiSanti *et al*. 1999). The spatial profile for a species released solely and uniformly at the nucleus, and expanding outward with constant velocity, should show a ρ^{-1} distribution ($\rho =$ projected distance from the nucleus). A species having a distributed contribution (e.g., CO) will fall off more slowly than ρ^{-1}. However, properties of the comet (e.g., outflow asymmetries) and observing conditions (primarily seeing and tracking errors) cause deviations from ρ^{-1} even in the absence of a distributed source (Dello Russo *et al*. 2000). For this reason, it is important to compare spatial profiles of volatiles and dust (simultaneously obtained), since seeing and drift will affect each in the same manner.

All HCN rovibrational lines sampled on a common day were summed and this partial band profile (e.g., 36% of the expected total band intensity on UT April 29.9) was compared with the profile of the (normalized) continuum emission (Fig. 5). The spatial profiles were examined to determine whether the distribution of HCN was characteristic of release at the nucleus alone or if release from a distributed source is also required. For all dates, the HCN profile is approximately east–west symmetric at all positions about the nucleus, while the continuum profiles reveal significant asymmetry (Figs. 1 and 5). The spatial distribution of a "parent" volatile released at the nucleus should be more isotropic than dust, owing to collisional effects (Combi 1996, Xie and Mumma 1996a, 1996b).

An effective "spherical" production rate (Q, molecules s^{-1}) may be derived from the intensity measured at a specific location,

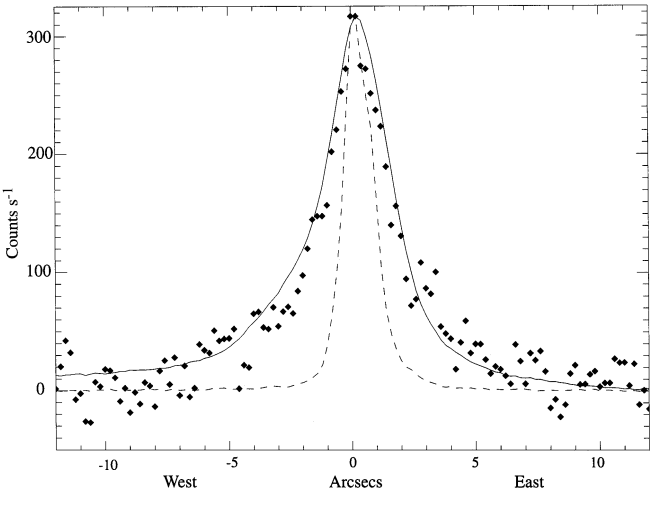

FIG. 5. Spatial profile of HCN, dust, and point spread function (star). The HCN profile (points) is east–west symmetric about its peak emission at all positions offset from the nucleus. The continuum profile (solid line, scaled to the peak of the cometary HCN profile) reveals significant asymmetry, being more extended toward the west (see Fig. 6B). The spatial profile of a star (dashed line) illustrates the point spread function, which was limited by seeing (FWHM $\sim 2''$). All profiles are normalized to a common value centered on the nucleus.

using the (idealized, but useful) assumption of uniform spherical outflow from the nucleus. A spherical production rate is obtained from

$$Q = \frac{4\pi\Delta^2 F}{(\mathrm{hc}\nu)g_1\tau_1 f(x)\beta},$$

where F is the measured partial band emission flux (W m^{-2}) at the top of the atmosphere, $f(x)$ is the fraction of the total HCN coma burden contained within the sampled region (Hoban *et al*. 1991), g_1 is the band fluorescence efficiency (3.88×10^{-4} photons s^{-1} molecule^{-1} at 1 AU, Varghese and Hanson 1984, Crovisier 1999, personal communication), β is the fraction of the band intensity contained within the measured lines, τ_1 is the lifetime of the HCN molecule (6.67×10^4 seconds at 1 AU, Bockelée-Morvan and Crovisier 1985), and hcν is the energy per photon (J). For projected distances much smaller than the scale length of HCN, this relation is nearly independent of the specific value of the lifetime. For an outflow velocity of 1.1 km/s (cf. Biver *et al*. 1999), the scale length is 7.3×10^4 km at 1 AU (corresponding to about 58 arcsec for geocentric distance of 1.753 AU).

The partial band intensity (F) is the sum of the measured individual line intensities within the aperture in question. The fraction β is obtained by band modeling using the measured rotational temperature of the (001) vibrational level (or an adopted one if too few lines were measured) and assuming that it reflects the rotational temperature of the (000) ground level. Chin and Weaver (1984) examined the relationship between the rotational population of the $v = 1$ and $v = 0$ vibrational levels of CO, using a model that included both collisional and radiative effects. They showed that the rotational distribution in $v = 1$ retains information from the rotational distribution of the ground level, since radiative rates dominate excitation and decay processes. As a result, the rotational population of the $v = 1$ is quite similar to that $v = 0$, and reflects the LTE distribution of the ground level.

We modeled the HCN populations in (001) and (000) vibrational levels by assuming a Boltzmann distribution in the ground vibrational level, and then used radiative excitation and decay rates for 30 rotational levels connecting the ground and excited vibrational states (Bockelée-Morvan and Crovisier 1985, Chin and Weaver 1984). The resulting rotational temperature in (001) was the same within 1 K to that in 000 at 120 K, the difference being less than the statistical uncertainty in our measured temperature. We thus calculate the individual line g factors using the measured rotational temperature of the (001) vibrational level and do not account for slight differences in the rotational temperature between the (000) and (001) vibrational levels.

We calculated a production rate from the summed emission profiles of the measured lines (ΣF_i) using the sum of their individual line g factors ($\beta g_{\mathrm{band}} = \Sigma g_i$). The fractional band intensity (β) represented by the sampled lines depends on the specific lines sampled and on the rotational temperature. We used band fractions based on the retrieved temperatures when available (Table III). On April 29.9, our retrieved rotational temperatures ranged from 95 K near the nucleus to 123 K at 3″ offset, and we adopted a temperature of 120 K at greater distances. For these eight lines, β is only weakly dependent on temperature—it decreases from 38 to 36% as the temperature increases from 95 to 120 K. For all other dates, β is only weakly dependent on rotational temperature (Table III) so production rates are not highly sensitive to the uncertainty in the adopted rotational temperature. Subtle differences between the retrieved rotational temperature of the (001) vibrational level and that assumed for the ground level would not significantly affect our derived HCN production rates.

Spherical production rates were evaluated for a 1″ × 1″ box at positions centered on the nucleus and stepped along the slit in increments of 1″ (Fig. 6A). Errors were estimated from the deviation of the spatial profile from a fitted Gaussian + polynomial profile. While we do not observe asymmetry in production rates for HCN, we take an east–west average to improve the signal to noise of the data. This "symmetrized" production rate increases from the nucleus-centered value to a terminal value at ~2000 km from the nucleus for both HCN and dust (Fig. 6C). The terminal value is taken as the total or "global" production rate, Q_{HCN} or Q_{dust}. We compare the global production rate (Q_{HCN}) with that for water obtained from direct measurements of the H_2O 100–010 band on common observation dates (Dello Russo *et al*. 2000). The weighted average of the relative abundance (HCN/H_2O) for the four dates of observation was (0.40 ± 0.05)%. HCN production rates, rotational temperatures, percent of band observed, partial band fluxes, and the measured abundance relative to water for all dates of observation are presented in Table III.

The initial off-nucleus increase of the production rate is also seen in related studies of other parent volatiles (DiSanti *et al*. 1999, Dello Russo *et al*. 1998, 2000). Possible reasons for this effect are discussed in Dello Russo *et al*. (1998), and include atmospheric seeing and drift of the comet in the slit. The effects of seeing are illustrated by generating a Q curve for a stellar profile convolved with a ρ^{-1} distribution (Fig. 6C). This Q curve also exhibits a similar increase in production rate until reaching a terminal value. Thus, seeing is probably the major reason why nuclear-centered extracts yield lowered production rates. The presence of an extended source would cause the Q curve for the volatile to reach its terminal value at even greater distances from the nucleus (depending on the spatial scale for its release) (cf. DiSanti *et al*. 1999).

DISCUSSION

The significance of HCN as an exogenous biogenic volatile is tied to its abundance and to its chemical form (monomer, addition polymer, oligomer) in comets. HCN mixing ratios appeared to vary greatly among comets (Bockelée-Morvan *et al*.

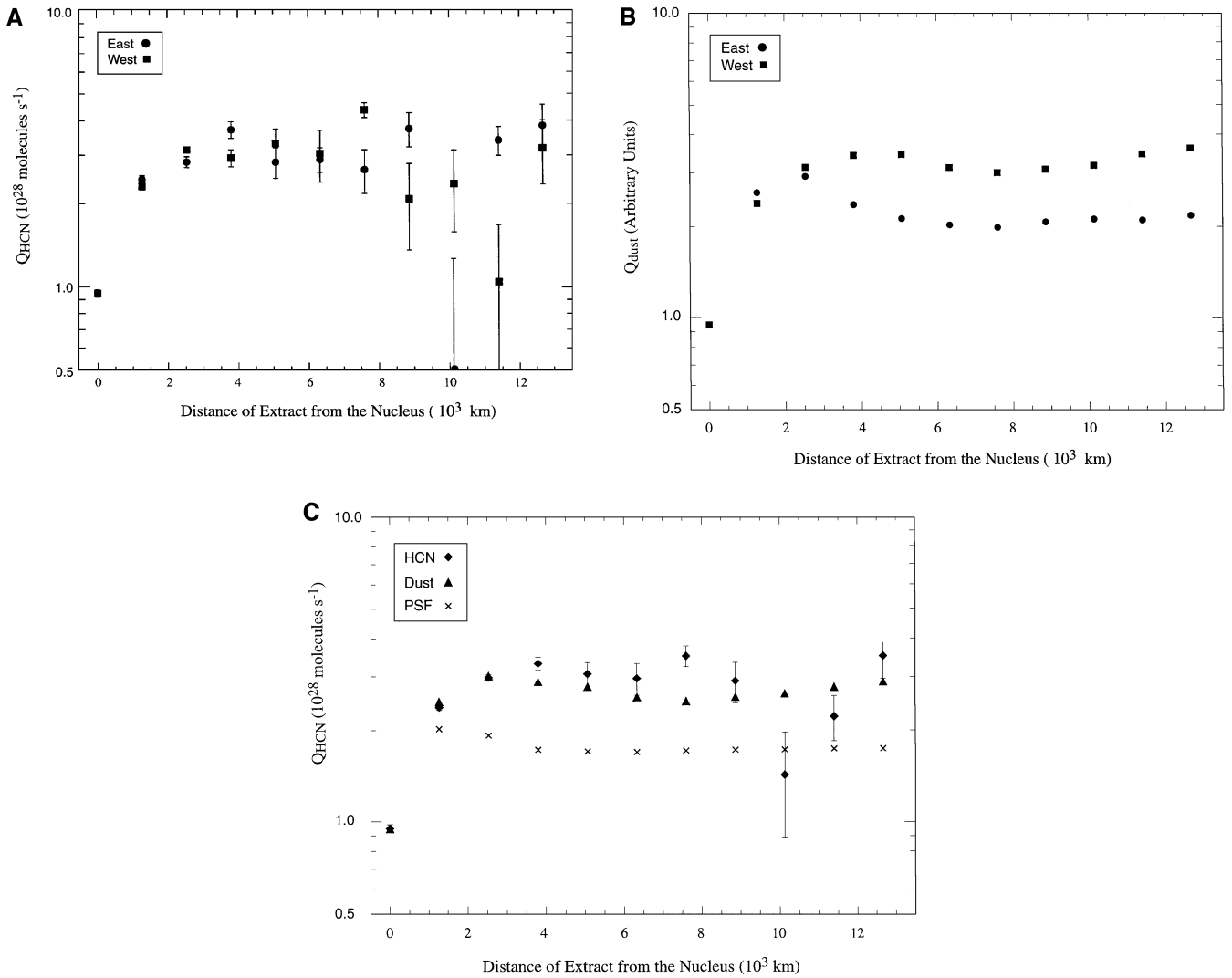

FIG. 6. Retrieved production rates for HCN in Comet Hale–Bopp on UT 1997 Apr 29.9. (A) Spherical production rates for HCN derived by stepping a $1'' \times 1''$ box using $1''$ steps east and west of the nucleus out to a distance of $10''$ (12,700 km). Comparison of east (circles) and west (squares) extracts reveals no significant asymmetry in HCN. (B) Spherical production rates for dust, east (circles) and west (squares) of the nucleus. The dust production rate was scaled to match the nucleus-centered production rate of HCN. The destruction scale length of dust was taken to be large compared with the spatial scale of the observations. A strong asymmetry favoring the sunward direction is seen. (C) Symmetrized production rates for HCN (diamonds) and dust (triangles), derived from a weighted average of east–west production rates. The effect of atmospheric seeing is illustrated by extracting symmetrized production rates from a synthetic spatial profile constructed by convolving the stellar PSF with a ρ^{-1} profile (x's).

1994), but a reanalysis by Biver (1997) with an improved model found HCN/H_2O to be around 0.1% for all comets measured except 109P Comet Swift Tuttle where the relative abundance was ∼0.25%. Wright *et al*. (1998) reanalyzed the detection claimed for Comet Kohoutek (Huebner *et al*. 1974) and obtained HCN/H_2O ∼4%. This value far exceeds that for any other comet, including Hale–Bopp. The relative abundance of HCN to H_2O measured by our group (∼0.40%) featured an internally consistent method for retrieving the respective production rates. Water production rates were obtained from direct measurements of three vibrational bands of H_2O obtained with the same instrument and analyzed with the same basic algorithms, using model parameters appropriate to water (Dello Russo *et al*. 2000).

Independent CSHELL observations of HCN on March 2–3 (Weaver *et al*. 1999) are probably consistent with our measurements if a common model and model parameters are used. Weaver *et al*. derive $Q_{HCN} = 8.5 \times 10^{27}$ molecules/s, based on spectral extracts ($1'' \times 2''$) centered on the nucleus, which we have demonstrated can underestimate the true production rate by a factor of ∼2–5, owing to seeing and guiding factors. To compare with our measurements, an additional correction (1.1/0.8) is needed since different outflow velocities were assumed. Based on the H_2O production rate measured on UT March 1.9 ($7.63 \pm 0.23 \times 10^{30}$ s^{-1}, Dello Russo *et al*. 2000) and our derived mixing ratio ($HCN/H_2O \sim 4.0 \times 10^{-3}$), we would expect $Q_{HCN} \sim 3 \times 10^{28}$ s^{-1} on UT March 1.9. It is not possible to derive an

exact universal scaling factor between our observations and those of Weaver *et al*. Seeing and guiding effects are variable for individual scans, and other modeling factors related to specific molecules are important as well. Considering these factors, the Weaver *et al*. measurements of Q_{HCN} on March 2–3 could be reconciled with our results.

Our absolute production rates for HCN are in agreement with those obtained from millimeter measurements by Womack *et al*. (1998), but are higher by a factor of two when compared to Biver *et al*. (1999) and Lovell *et al*. (1998) for common dates. However, direct comparison of absolute and relative production rates obtained by different groups can be misleading. Agreement of absolute production rates might be more coincidental than consistent when observing approach, beam sizes, model parameters (outflow velocity, lifetimes, etc.), and model complexity differ.

Our measured spatial distribution for HCN is consistent with its release at the nucleus—no significant contribution from a distributed source is required. Spherical production rates for HCN reveal no significant asymmetry (Fig. 6A). This is contrary to the case for dust (Fig. 6B), which exhibits an asymmetric dust production favoring the sunward direction. Despite the fact that Hale–Bopp is the dustiest comet known, there is no evidence that addition polymers or grains contribute a significant extended source for HCN monomers in Comet Hale–Bopp within 10,000 km of the nucleus. Our results show that the high mixing ratio of HCN in Hale–Bopp is not causally related to the grains seen at optical wavelengths. Our data do not test the presence of oligomers of HCN, since these would release NH_2, CN, and C_2 upon dissociation, but not HCN monomers. Regardless, HCN is present in Hale–Bopp in greater abundance than in most other comets, and our results suggest that most if not all of this HCN is present as a nuclear ice.

Wright *et al*. (1998) mapped HCN in Hale–Bopp with the BIMA interferometric array. They compared azimuthally averaged profiles with Haser models, inferring that up to 20% could be produced from a distributed source at distances greater than 10″. However, small contributions from coma chemistry (Irvine *et al*. 1998, Rodgers and Charnley 1998) or temporal variability (Wright *et al*. 1998) could help account for the deviation from a Haser profile of a native parent. We find no evidence for a distributed source within 10″ of the nucleus, however our data have insufficient sensitivity to confirm or rule out a small contribution from an extended source outside of 10″ from the nucleus (>12,000 km on April 29.9).

Jets of CN were discovered in Comet Halley (A'Hearn *et al*. 1986, Cosmovici *et al*. 1988). These were distinct from dust jets seen at optical wavelengths, leading to the suggestion that some CN is released from very small organic grains such as the CHON particles found in that comet. Alternately, Combi (1987) suggested that a gaseous parent of CN was confined in a jet by the general coma gas. Klavetter and A'Hearn (1994) revisited this problem and concluded that ∼50% of CN was released in these jets, the remainder being released isotropically (all CN is released from distributed sources). We see no evidence for jets of HCN in Hale–Bopp; however, long slit spectroscopy is not the optimum mode to study jets since detection depends on overlap of the slit with the jet.

The production rate for CN obtained 1997 May 1 (near the time of our HCN observations of Apr 29.9) was about 1×10^{28} molecules/s measured with an aperture 20–30″ in diameter (Schleicher 1999, personal communication), or ∼1/3 of our production rate for HCN. Photo dissociation of HCN by solar radiation produces CN with ∼97% efficiency (Huebner *et al*. 1992), so our measured production rate for HCN is more than adequate to provide the CN observed—indeed, some CN is "missing." The reasons for this discrepancy are not yet resolved, but are at least partly related to the scalelengths used in the Haser model to derive CN production rates. The abundance of HCN is large enough to account for the entire retrieved production of CN, however the spatial profile of the CN emission may not match with an HCN parent (Festou *et al*. 1998). If this were so, an alternate destruction mechanism would be needed for HCN—one that does not release CN. Evaluation of other potential sources for CN (e.g., other volatiles or grains) must await revised modeling of CN production rates and measurements of the spatial distributions for CN and its potential parents in Comet Hale–Bopp (Festou *et al*. 1998, Woodney *et al*. 1998).

The average rotational temperature retrieved for the (001) level in the intermediate coma (4″–10″ off the nucleus) for HCN (122 ± 8) K is slightly higher than that for CO (106 K ± 3 K in a region 4″–11″ off the nucleus, DiSanti *et al*. 1999) for the UT 1997 April 29.9 observations. An even lower temperature was retrieved for H_2O (77 K, $+11 - 8$ K, in a region 2″–12″ off the nucleus) on the same day (April 29.9) using the same instrument and common observing and analysis techniques (Dello Russo *et al*. 2000). These differences likely reflect rotational excitation and relaxation probabilities for the individual species, which are controlled by dipole moments both for radiative cooling and for collisional excitation by electrons (Xie and Mumma 1992). The rotational temperature for HCN increases with cometocentric distance, similar to the behavior found for CO (DiSanti *et al*. 1999). Measurements of rotational temperatures in the ground vibrational level for other molecules at similar heliocentric distance are consistent with the HCN and CO results (e.g., 103 ± 7 K for CH_3OH and CO, Biver *et al*. 1999), but a detailed comparison is difficult because of observational and modeling differences.

The measurement of spatially resolved rotational temperatures for cometary volatiles provides a new and useful tool for studies of heating in the inner coma. With CSHELL, rotational temperatures can be sampled with just a few grating settings. This technique will advance dramatically with the use of cross-dispersed instruments currently being developed. These will permit spectrally resolved molecular bands to be sampled in a single exposure, enabling study of variable production rates and coma phenomena with greatly improved temporal resolution.

Additional work is needed to link the spatial character of HCN emission and its production rate with that of its proposed daughter products. Our group's set of infrared detections in Comet Hale–Bopp and Comet Hyakutake includes emissions

from many species linked to this question (NH_3, NH_2, CN, for example) and will be used to further test the nature of HCN in comets.

ACKNOWLEDGMENTS

This work was supported by the National Science Foundation RUI Grant AST-9619461, NASA JOVE program, Rowan University, and the NASA Planetary Astronomy Program under RTOP 344-32-30-07. We are grateful to the outstanding support from the staff of the NASA Infrared Telescope Facility. The University of Hawaii under contract to NASA operates the NASA IRTF. KM-S thanks Rowan University undergraduate Kim D. Ha for her assistance in this project.

REFERENCES

A'Hearn, M. F., S. Hoban, P. V. Birch, C. Bowers, R. Martin, and D. A. Klinglesmith, III 1986. Cyanogen jets in Comet Halley. *Nature* **324**, 649–651.

Biver, N. 1997. *Molécules mères cométaires: Observations et modélisations*. Ph.D. thesis, Université Paris.

Biver, N., and 11 colleagues 1997. Evolution of the outgassing of Comet Hale–Bopp. *Science* **275**, 1915–1917.

Biver, N., and 22 colleagues 1999. Long term evolution of the outgassing of Comet Hale–Bopp (C/1995 O1) from radio observations. *Earth Moon Planets*, in press.

Bockelée-Morvan, D., and J. Crovisier 1985. Possible parents for the cometary CN radical: Photochemistry and excitation conditions. *Astron. Astrophys*. **151**, 90–100.

Bockelée-Morvan, D., and J. Crovisier 1987. The 2.7 μm water band of Comet P/Halley: Interpretation of observations by an excitation model. *Astron. Astrophys*. **187**, 425–430.

Bockelée-Morvan, D., J. Crovisier, A. Baudry, D. Despois, M. Perault, W. M. Irvine, F. P. Schloerb, and D. Swade 1984. Hydrogen cyanide in comets—Excitation conditions and radio observations of Comet IRAS-Araki-Alcock 1983d. *Astron. Astrophys*. **141**, 411–418.

Bockelée-Morvan, D., J. Crovisier, P. Colom, D. Despois, and G. Paubert, 1990. Observations of parent molecules in Comets P/Brorsen-Metcalf (1989o), Austin (1989cl), and Levy (1990c) at millimeter wavelengths: HCN, H_2S, H_2CO, and CH_3OH. In *Proc. 24th ESLAB Symp. on Formation of Stars and Planetary*, ESA SP-315, pp. 143–148.

Bockelée-Morvan, D., J. Crovisier, D. Despois, T. Foreville, E. Gerard, J. Schraml, and C. Thum 1986. A search for parent molecules at millimeter wavelengths in Comets P/Giacobini-Zinner 1994e and P/Halley 1982i. In *Proceedings of the 20th ESLAB Symposium on the Exploration of Halley's Comet*, Vol. 1, pp. 365–367.

Bockelée-Morvan, D., J. Crovisier, D. Despois, T. Foreville, E. Gerard, J. Schraml, and C. Thum, 1987. Molecular observations of Comets P/Giacobini-Zinner 1984e and P/Halley 1982i at millimetre wavelengths. *Astron. Astrophys*. **180**, 253–262.

Bockelée-Morvan, D., R. Padman, J. K. Davies, and J. Crovisier 1994. Observations of submillimetre lines of CH_3OH, HCN, and H_2CO in Comet P/Swift–Tuttle with the James Clerk Maxwell Telescope. *Planet. Space Sci*. **42**, 665–662.

Bockelée-Morvan, D., J. Wink, D. Despois, N. Biver, P. Colom, J. Crovisier, E. Gerard, E. Lellouch, and L. Jorda 1998. Interferometric imaging of molecular lines in Comet Hale–Bopp. *Bull. Am. Astron. Soc*. **30**(31.02).

Bockelée-Morvan, D., and 14 colleagues 1999. A molecular survey of Comet C/1995 O1 (Hale–Bopp) at the IRAM telescopes. *Earth Moon Planets*, in press.

Boss, A. P. 1998. Temperatures in protoplanetary disks. *Annu. Rev. Earth Planet. Sci*. **26**, 53–80.

Brooke, T. Y., A. T. Tokunaga, H. A. Weaver, J. Crovisier, D. Bockelée-Morvan, and D. Crisp 1996. Detection of acetylene in the infrared spectrum of Comet Hyakutake. *Nature* **383**, 606–608.

Brooke, T. Y., H. A. Weaver, G. Chin, and S. J. Kim 1998. Spectroscopy of Comet Hale–Bopp in the infrared. *Bull. Am. Astron. Soc*. **30**(31.12).

Chin, G., and H. A. Weaver 1984. Vibrational and rotational excitation of CO in comets: Nonequilibrium calculations. *Astrophys. J*. **285**, 858–869.

Chyba, C. F., and C. Sagan 1992. Endogenous production, exogenous delivery, and impact-shock synthesis of organic molecules: An inventory for the origins of life. *Nature* **355**, 125–132.

Chyba, C. F., T. C. Owen, and W.-H. Ip 1994. Impact delivery of volatiles and organic molecules to Earth. In *Hazards Due to Comets and Asteroids* (T. Gehrels, Ed.), pp. 9–59. Univ. of Arizona Press, Tucson.

Clemett, S. J., C. R. Maechling, R. N. Zare, P. D. Swan, and R. M. Walker 1993. Identification of complex aromatic molecules in individual interplanetary dust particles. *Science* **262**, 721–725.

Combi, M. R. 1987. Sources of cometary radicals and their jets: Gases or grains? *Icarus* **71**, 178–191.

Combi, M. R. 1996. Time-dependent gas kinetics in tenuous planetary atmospheres: The cometary coma. *Icarus* **123**, 207–226.

Cosmovici, C. B., G. Schwarz, W.-H. Ip, and P. Mack 1988. Gas and dust jets in the inner coma of Comet Halley. *Nature* **332**, 705–709.

Cronin, J. R., and S. Chang, 1993. Organic matter in meteorites: Molecular and isotopic analyses of the Murchison meteorite. In *Chemistry of Life's Origins* (J. M. Greenberg, C. X. Mendozo-Gomez, and V. F. Pironello, Eds.), pp. 205–258. Kluwer Academic Press, Dordrecht.

Crovisier, J. 1987. Synthetic spectra of linear parent molecules in comets. *Astron. Astrophys. Suppl*. **68**, 223–258.

Crovisier, J., D. Bockelée-Morvan, P. Colom, D. Despois, and G. Paubert 1993. A search for parent molecules at millimetre wavelengths in Comets Austin 1990 V and Levy 1990 XX—Upper limits for undetected species. *Astron. Astrophys*. **269**(1–2), 527–540.

Dello Russo, N., M. A. DiSanti, M. J. Mumma, K. Magee-Sauer, and T. W. Rettig 1998. Carbonyl sulfide in Comets C/1996 B2 (Hyakutake) and C/1995 O1 (Hale–Bopp): Evidence for an extended source in Hale–Bopp. *Icarus* **135**, 377–388.

Dello Russo, N., M. J. Mumma, M. A. DiSanti, K. Magee-Sauer, R. Novak, and T. W. Rettig 2000. Water production and release in Comet C/1995 O1 (Hale–Bopp). *Icarus*, in press.

Despois, D. 1999. Radio observations of molecular and isotopic species: Implications on the interstellar origin of cometary ices. *Earth Moon Planets*, in press.

Despois, D., J. Crovisier, D. Bockelèe-Morvan, J. Schraml, T. Forveille, and E. Gerard, 1986. Observations of hydrogen cyanide in Comet Halley. *Astron. Astrophys.* **160**, L11–L12.

DiSanti, M. A., M. J. Mumma, N. Dello Russo, K. Magee-Sauer, R. Novak, and T. W. Rettig 1999. Identification of two sources for carbon monoxide in Comet Hale–Bopp. *Nature* **399**, 662–665.

Ferris, J. P., and W. J. Hagan 1984. HCN and chemical evolution: The possible role of cyano compounds in prebiotic synthesis. *Tetrahedron* **40**, 1093–1120.

Festou, M. C., O. Barale, T. Davidge, S. A. Stern, G. P. Tozzi, M. Womack, and J. M. Zucconi 1998. Tentative identification of the parent of CN radicals in comets: C_2N_2. *Bull. Am. Astron. Soc*. **30**(40.02).

Greene, T. P., A. T. Tokunaga, D. W. Toomey, and J. S. Carr 1993. CSHELL: A high spectral resolution 1–5 micron cryogenic echelle spectrograph for the IRTF. *Proc. SPIE* **1946**, 311.

Herzberg, G. 1950. *Spectra of Diatomic Molecules*, p. 126. Van Nostrand–Reinhold, New York.

Hoban, S., M. J. Mumma, D. C. Reuter, M. DiSanti, R. R. Joyce, and A. Storrs 1991. A tentative identification of methanol as the progenitor of the 3.52 μm feature in several comets. *Icarus* **93**, 122–134.

Huebner, W. F., D. C. Boice, and A. Korth 1989. Halley's polymeric organic molecules. *Adv. Space Res*. **9**, 29–34.

Huebner. W. F., J. J. Keady, and S. P. Lyon 1992. Solar photorates for planetary atmospheres and atmospheric pollutants. *Astrophys. Space Sci*. **195**, 1–294.

Huebner, W. F., L. E. Snyder, and D. Buhl 1974. HCN radio emission from Comet Kohoutek (1973f). *Icarus* **23**, 580–585.

Irvine, W. M., and 39 colleagues 1984. Radioastronomical observations of Comets IRAS–Araki–Alcock (1983d) and Sugano–Saigusa–Fujikawa (1983e). *Icarus* **60**, 215–220.

Irvine, W. M., J. E. Dickens, A. J. Lovell, F. P. Schloerb, M. Senay, E. A. Bergin, D. Jewitt, H. E. Matthews 1998. Chemistry in cometry comae. *Faraday Discuss*. **109**, 475.

Klavetter, J. J., and M. F. A'Hearn 1994. An extended source for CN jets in Comet P/Halley. *Icarus* **107**, 322–334.

Kunde, V. G., and J. C. Maguire 1974. Direct integration transmittance model. *J. Quant. Spectrosc. Radiat. Trans*. **14**, 803–817.

Lis, D. C., J. Keene, K. Young, T. G. Phillips, D. Bockelée-Morvan, J. Crovisier, P. Schilke, P. F. Goldsmith, and E. A. Bergin 1997. Spectroscopic observations of Comet C1996 B2 (Hyakutake) with the Caltech Submillimeter Observatory. *Icarus* **130**, 355–372.

Lovell, A. J., F. P. Schloerb, J. E. Dickens, C. H. Devries, W. M. Irvine, and M. C. Senay 1998. Molecular line mapping of Comets Hyakutake and Hale–Bopp. *Bull. Am. Astron. Soc*. **30**, No. 31.15.

Magee-Sauer, K., M. J. Mumma, M. A. DiSanti, N. Dello Russo, T. Rettig, and R. Novak 1997. Infrared spectroscopy of the 3.0 μm region: Observations with CSHELL of C/1995 O1 Hale–Bopp. *Bull. Am. Astron. Soc*. **29**, No. 34.01.

Magee-Sauer, K., M. J. Mumma, M. A. DiSanti, N. Dello Russo, and T. Rettig 1998. CSHELL observations of HCN, C_2H_2, and NH_3 in Comets 1995 O1 (Hale–Bopp) and 1996 B2 Hyakutake. *Bull. Am. Astron. Soc*. **30**, No. 29.12.

Matthews, C. N., and R. Ludicky 1992. Hydrogen cyanide polymers on comets. *Adv. Space Res*. **12**, 21–32.

McKay, C. P. 1991. Urey Prize lecture: Planetary evolution and the origin of life. *Icarus* **91**, 93–100.

Mumma, M. J. 1997. Organic volatiles in comets: Their relation to interstellar ices and solar nebula material. In *From Stardust to Planetesimals* (Y. Pendleton and A. G. G. M. Tielens, Eds.), Astronomical Society of the Pacific Conf. Series, No. 122, pp. 369–396.

Mumma, M. J., P. R. Weissman, and S. A. Stern 1993. Comets and the origin of the Solar System: Reading the Rosetta Stone. In *Protostars and Planets III* (E. H. Levy and J. I. Lunine, Eds.), pp. 1177–1252. Univ. Arizona Press, Tucson.

Mumma, M. J., M. A. DiSanti, N. Dello Russo, M. Fomenkova, K. Magee-Sauer, C. D. Kaminski, and D. X. Xie 1996. Detection of abundant ethane and methane, along with carbon monoxide and water, in Comet C/1996 B2 Hyakutake: Evidence for processed interstellar ice. *Science* **272**, 1310–1314.

Oro, J. 1961. Comets and the formation of biochemical compunds on the primitive Earth. *Nature* **190**, 389–390.

Oro, J., T. Mills, and A. Lazcano 1992. Comets and the formation of biochemical compounds on the primitive Earth—A review. *Origins of Life* **21**, 267–277.

Palmer, P., M. F. A'Hearn, I. DePater, J. J. Klavetter, D. Mehringer, F. P. Schloerb, L. E. Snyder, and D. Wilner 1990. Simultaneous imaging of optical CN lines and radio HCN lines in Comet Austin. In *Workshop on Observations of Recent Comets*, pp. 40–44. Southwest Research Institute.

Pauling, L. 1960. *The Nature of the Chemical Bond*. Cornell Univ. Press, Ithaca.

Pimentel, G. C., and A. L. McClellan 1960. *The Hydrogen Bond*. Freeman, San Francisco.

Rauer, H., and 11 colleagues 1996. The evolution of the outgassing of Comet C/1995 O1 (Hale–Bopp) from radio observations. *Bull. Am. Astron. Soc*. **28**, No. 09.20.

Rettig, T. W., S. C. Tegler, D. J. Pasto, and M. J. Mumma 1992. Comet outbursts and polymers of HCN. *Astrophys. J*. **398**, 293–298.

Rodgers, S. D., and S. B. Charnley 1998. HNC and HCN in comets. *Astrophys. J*. **501**, L227–L230.

Rothman, L. S., and 13 colleagues 1992. The HITRAN molecular database: Editions of 1991 and 1992. *J. Quant. Spectrosc. Radiat. Transfer* **48**, 469–507.

Schloerb, F. P., W. M. Kinzel, D. A. Swade, and W. M. Irvine, 1987. Observations of HCN in Comet Halley. *Astron. Astrophys*. **187**, 475–480.

Schloerb, F. P., A. J. Lovell, J. E. Dickens, C. H. Devries, and W. M. Irvine 1996. Mapping of HCN in the coma of Comet C/1996 B2 Hyakutake. *Bull. Am. Astron. Soc*. **28**, No. 09.19.

Schulze, H., J. Kissel, and E. K. Jessberger 1997. Chemistry and mineralogy of Comet Halley's dust. In *From Stardust to Planetesimals* (Y. Pendleton and A. G. G. M. Tielens, Eds.), Astronomical Society of the Pacific Conf. Series, No. 122, pp. 397–414.

Varghese, P. L., and R. K. Hanson 1984. Tunable diode laser measurements of spectral parameters of HCN at room temperature. *J. Quant. Spectrosc. Radiat.Trans*. **31**, 545–559.

Veal, J. M., L. E. Synder, I. De Pater, M. C. H. Wright, J. R. Forster, P. Palmer, L. M. Woodney, M. F. A'Hearn, and Y.-J. Kuan 1998. BIMA array observations of Comet Hale–Bopp: Evidence of deviations from spherical outflow. *Bull. Am. Astron. Soc*. **192**, No. 08.03.

Völker, T. 1960. Polymeric hydrogen cyanide. *Angew. Chemic* **72**, 379–384.

Weaver, H. A., T. Y. Brooke, G. Chin, S. J. Kim, D. Bockelée-Morvan, and J. K. Davies 1999. Infrared spectroscopy of Comet Hale–Bopp. *Earth Moon Planets*, in press.

Winnberg, A., L. Ekelund, and A. Ekelund 1987. Detection of HCN in Comet P/Halley. *Astron. Astrophys*. **172**, 335–341.

Womack, M., M. C. Festou, and S. A. Stern 1998. The heliocentric evolution of carbon-bearing volatiles in Comet Hale–Bopp. *Bull. Am. Astron. Soc*. **30**, No. 31.11.

Woodney, L. M., and 11 colleagues 1998. Morphology of HCN and CN in Comet Hale–Bopp. *Bull. Am. Astron. Soc*. **30**, No. 31.03.

Wootten, A., W. B. Latter, and D. Despois 1994. HCN emission from Comet P/Swift–Tuttle 1992t. *Planet. Space Sci*. **42**, 727–731.

Wright, M. C. H., I. de Pater, J. R. Foster, P. Palmer, L. E. Snyder, J. M. Veal, M. F. A'Hearn, L. M. Woodney, W. M. Jackson, Y.-J. Kuan, and A. J. Lovell 1998. Mosaiced images and spectra of J = 1-0 HCN and HCO^+ emission from Comet Hale–Bopp (1995 O1). *Astron. J*. **116**, 3018–3028.

Xie, D. X., and M. J. Mumma, 1992. The effect of electron collisions on rotational populations of cometary water. *Astrophys. J*. **386**, 720–728.

Xie, D. X., and M. J. Mumma 1996a. Monte Carlo simulation of cometary atmospheres: Application to Comet P/Halley at the time of the Giotto spacecraft encounter. I. Isotropic Model. *Astrophys. J*. **464**, 442–456.

Xie, D. X., and M. J. Mumma 1996b. Monte Carlo simulation of cometary atmospheres: Application to Comet P/Halley at the time of the Giotto spacecraft encounter. II. Axi-symmetric Model. *Astrophys. J*. **464**, 457–475.